



The identification, analysis and structure-based development of novel inhibitors of 6-hydroxymethyl-7,8-dihydropterin pyrophosphokinase



Mi-Kyung Yun^a, Daniel Hoagland^b, Gyanendra Kumar^a, M. Brett Waddell^a, Charles O. Rock^{c,d}, Richard E. Lee^{b,d,*}, Stephen W. White^{a,d,*}

^a Department of Structural Biology, St. Jude Children's Research Hospital, Memphis, TN 38105, USA

^b Department of Chemical Biology and Therapeutics, St. Jude Children's Research Hospital, Memphis, TN 38105, USA

^c Department of Infectious Diseases, St. Jude Children's Research Hospital, Memphis, TN 38105, USA

^d Department of Microbiology, Immunology and Biochemistry, University of Tennessee Health Science Center, Memphis, TN 38163, USA

ARTICLE INFO

Article history:

Received 31 December 2013

Revised 4 February 2014

Accepted 14 February 2014

Available online 25 February 2014

Keywords:

Antimicrobial

HPPK

Pterin

Folate

X-ray crystallography

ABSTRACT

6-Hydroxymethyl-7,8-dihydropterin pyrophosphokinase (HPPK) is an essential enzyme in the microbial folate biosynthetic pathway. This pathway has proven to be an excellent target for antimicrobial development, but widespread resistance to common therapeutics including the sulfa drugs has stimulated interest in HPPK as an alternative target in the pathway. A screen of a pterin-biased compound set identified several HPPK inhibitors that contain an aryl substituted 8-thioguanine scaffold, and structural analyses showed that these compounds engage the HPPK pterin-binding pocket and an induced cryptic pocket. A preliminary structure activity relationship profile was developed from biophysical and biochemical characterizations of derivative molecules. Also, a similarity search identified additional scaffolds that bind more tightly within the HPPK pterin pocket. These inhibitory scaffolds have the potential for rapid elaboration into novel lead antimicrobial agents.

© 2014 Elsevier Ltd. All rights reserved.

1. Introduction

A number of key metabolic reactions, such as the synthesis of thymine, involve a one-carbon transfer step, and the carbon atom is supplied by the essential cofactor tetrahydrofolate.¹ Higher organisms derive folate from their diet as vitamin B9, but the vast majority of eubacteria and many lower eukaryotes synthesize tetrahydrofolate de novo. The folate biosynthetic pathway is therefore an ideal target for the development of antibiotics.² This is exemplified by the sulfonamide class of drugs (sulfa drugs) that target the enzyme dihydropteroate synthase (DHPS) in the pathway. Sulfa drugs have remained important broad spectrum clinical agents

since their discovery 80 years ago,³ but their use has been seriously compromised by widespread microbial resistance and severe allergic reactions.

We recently showed that DHPS from the pathogen *Francisella tularensis* is part of a bifunctional enzyme and fused to 6-hydroxymethyl-7,8-dihydropterin pyrophosphokinase (HPPK) that catalyzes the previous step in the pathway.⁴ We also showed that one of our DHPS pterin-pocket inhibitors engages the HPPK pterin pocket, even though there is no structural similarity between the pockets. Despite its high conservation and pivotal role in folate synthesis, there have been relatively few attempts to develop lead inhibitory compounds against HPPK as potential novel antibiotics.^{5–7} This is somewhat surprising because many HPPK crystal structures are now available^{4,5,8–11} and the catalytic mechanism is understood.^{6,7,12–18} This untapped potential has been noted,¹⁹ and there has recently been renewed interest in HPPK as an antimicrobial drug target.^{20–23}

HPPK is a small (~18 kDa) highly conserved enzyme with an $\alpha\beta$ fold that catalyzes the transfer of pyrophosphate from ATP to 6-hydroxymethyl-7,8-dihydropterin (DHP) to form 6-hydroxymethyl-7,8-dihydropterin-pyrophosphate (DHPPP), one of the two substrates of DHPS. The adenosine ring of ATP packs into a

Abbreviations: HPPK, 6-hydroxymethyl-7,8-dihydropterin pyrophosphokinase; DHP, 6-hydroxymethyl-7,8-dihydropterin; DHPS, dihydropteroate synthase; SPR, surface plasmon resonance; K_D , equilibrium dissociation constant; IC_{50} , half maximal inhibitory concentration; AMPCPP, α,β -methyleneadenosine 5'-triphosphate; EchHPPK, *Escherichia coli* 6-hydroxymethyl-7,8-dihydropterin pyrophosphokinase; BME, 2-mercaptoethanol.

* Corresponding authors. Tel.: +1 901 595 6617; fax: +1 901 595 5715 (R.E.L.); tel.: +1 901 595 3040; fax: +1 901 595 3032 (S.W.W.).

E-mail addresses: richard.lee@stjude.org (R.E. Lee), stephen.white@stjude.org (S.W. White).

conserved cleft, the triphosphate is coordinated by two essential Mg^{2+} ions, and DHP binds within an adjacent pocket with the pterin ring π -stacked between two conserved aromatic residues. HPPK uses an ordered enzyme mechanism in which the ATP cleft is first occupied, followed by the binding of DHP. Similar to DHPS,²⁴ HPPK uses stabilizing loop conformational changes to assemble the complete active site and the DHP binding pocket.^{13,17,25,26}

Our discovery that a DHPS pterin-pocket inhibitor can also engage the pterin pocket of *F. tularensis* HPPK (FtHPPK) is not altogether surprising because the product of HPPK, DHP, is the substrate for DHPS, and the architectures of both pockets have therefore evolved to engage the same small molecule. This observation prompted us to screen our library of DHPS pterin-pocket binding molecules for additional HPPK inhibitors. These studies yielded two related compounds, and using a structure-based approach, we have synthesized derivative compounds and derived an initial SAR pattern. Based on these data, we then performed a similarity search of the NCI compound repository, and identified and structurally characterized several inhibitory fragment scaffolds for future optimization.

2. Results

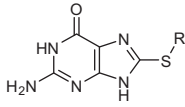
2.1. Initial screen of DHPS pterin pocket inhibitors

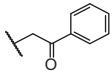
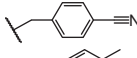
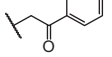
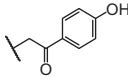
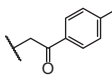
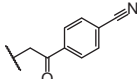
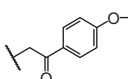
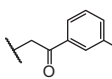
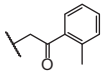
During the course of our drug discovery studies on DHPS, we have generated a library of ~230 potential pterin pocket binding molecules. Using an endpoint HPPK assay that monitors unprocessed ATP substrate as a direct readout of inhibition, we screened these compounds against *Escherichia coli* HPPK (EchHPPK). The screen revealed 2 compounds that significantly inhibit HPPK at 250 μM (compounds **1** and **2**, Table 1). To characterize the binding of **1** and **2** to EchHPPK in more detail, we used surface plasmon resonance (SPR) to measure their binding characteristics. EchHPPK was immobilized on the sensor chip, and binding was measured in the absence and presence of 2 μM of the non-hydrolysable ATP analog AMPCPP. The sensorgrams and binding isotherms are shown in Figures S1a and S1b, and it is clear that the compounds showed no appreciable binding in the absence of AMPCPP but robust binding in the presence of AMPCPP. In the HPPK enzyme mechanism, the assembly of the pterin-binding pocket depends on ATP-dependent conformational changes in the three active site loops,¹³ and the SPR data are therefore consistent with **1** and **2** both engaging the pterin pocket. The rapid dissociation rates (k_d) of **1** and **2** precluded the measurement of K_D values using the SPR kinetic approach, but it was possible to obtain the K_D values using the alternative equilibrium affinity method, and these are shown in Table 1. We also used the identical SPR protocol to measure the K_D of DHP (Table 1, Fig. S2), and this confirmed that **1** and **2** represent weak initial hit molecules that require significant optimization to efficiently compete with the HPPK pterin substrate. Note that it was possible to measure the K_D of DHP by SPR using the kinetic approach, and the value agrees well with that obtained by the equilibrium affinity method ($1.31 \pm 0.03 \mu M$ K_D (eq) versus $1.05 \pm 0.01 \mu M$ K_D (kin); Fig. S2). Note also that our measured K_D for DHP is significantly higher than that previously reported by Li et al.¹⁵ but we attribute this discrepancy to the much lower concentration of AMPCPP used in our experiment (2 μM vs 100 μM). Isothermal titration calorimetry experiments (not shown) support this explanation.

2.2. The 8-thioguanine scaffold

Compounds **1** and **2** both contain an 8-alkylated-8-thioguanine scaffold, and its ability to mediate the inhibition of EchHPPK is consistent with similar studies on *Staphylococcus aureus* HPPK

Table 1
Compound **1** variants



Compound	R	% Inhibition ^a	K_D^b (μM)	IC ₅₀ (μM)
1		75	9.7 ± 0.4	139
2		53	29 ± 2	254
3		80	6.7 ± 0.2	64
4		77	5.8 ± 0.2	82
5		73	11.2 ± 0.5	79
6		68	39 ± 3	88
7		74	14.5 ± 0.6	44
8		77	5.9 ± 0.3	51
9		48	18.9 ± 0.9	243
10 DHP ^c		18	>100 1.31 ± 0.03	

^a % Inhibition of enzyme activity was tested at 250 μM of the compound.

^b K_D value was determined by SPR with equilibrium affinity analysis in the presence of 2 μM AMPCPP.

^c The pterin substrate of HPPK, 6-hydroxymethyl-7,8-dihydropterin.

(SaHPPK).²⁰ Those studies included structural characterizations using X-ray crystallography which revealed that free 8-thioguanine is sandwiched between the two conserved aromatic side chains with the ring oxygen and nitrogen atoms engaging in hydrogen bonding interactions similar to those of the natural pterin substrate. However, compounds **1** and **2** appear to be more potent than either 8-thioguanine itself or derivatives that were recently reported.²³ We therefore analyzed their ternary complexes with AMPCPP by X-ray crystallography to understand the structural basis of this potency. EchHPPK forms high quality crystals in well characterized conditions,⁸ and it was possible to obtain high resolution structures for both ternary complexes (Table 2, Table S1, Fig. 1, Fig. S3). It should be noted that the crystallization conditions for **1** and **2** contain 0.2 M $CaCl_2$, and based on the high quality refined electron density (Fig. S4), it was apparent that Ca^{2+} ions had replaced Mg^{2+} ions at the active site. However, the two-metal site is not part of the pterin pocket, and this crystallization artifact does not appear to impact the binding of these compounds or those described later in this study. The identity of the metals in each of the structures is noted in Tables S1 and S2.

Overall, both structures are very similar to that of the previously reported HPPK-AMPCPP-DHP substrate ternary complex,¹³ and Figure 1a shows a detailed stereo view of the compound **1** ternary complex. The 8-thioguanine scaffold occupies the pterin

Table 2
Summary of crystallographic refinement data

Compound	Space group	Cell dimensions		Resolution range (Å)	$R_{\text{work}}/R_{\text{free}}^a$	PDB accession code ^b
		a, b, c (Å)	α, β, γ (°)			
1	P2 ₁	35.9, 57.4, 38.3	90.0, 114.0, 90.0	22.2–1.3	0.144/0.177	4M5G
2	P2 ₁	35.8, 57.6, 38.5	90.0, 115.4, 90.0	32.3–1.1	0.134/0.149	4M5H
3	P2 ₁	35.9, 58.1, 38.4	90.0, 115.6, 90.0	34.7–1.1	0.152/0.167	4M5I
7	P2 ₁	36.5, 58.4, 38.4	90.0, 113.8, 90.0	33.4–1.7	0.168/0.213	4M5J
8	P2 ₁	36.0, 57.9, 38.5	90.0, 115.4, 90.0	34.8–1.3	0.149/0.174	4M5K
9	P2 ₁	35.9, 58.0, 38.6	90.0, 115.5, 90.0	19.9–1.1	0.173/0.186	4M5L
18	P2 ₁	35.9, 57.9, 38.7	90.0, 115.6, 90.0	34.9–1.1	0.170/0.191	4M5M
21	P3 ₁	107.3, 107.3, 41.8	90.0, 90.0, 120.0	35.1–2.0	0.159/0.192	4M5N

^a R_{free} is the R value obtained for a test set of reflections consisting of randomly selected 5% subset of the data set excluded from refinement.

^b Coordinates and structure factors for all the structures have been deposited in the Protein Data Bank.

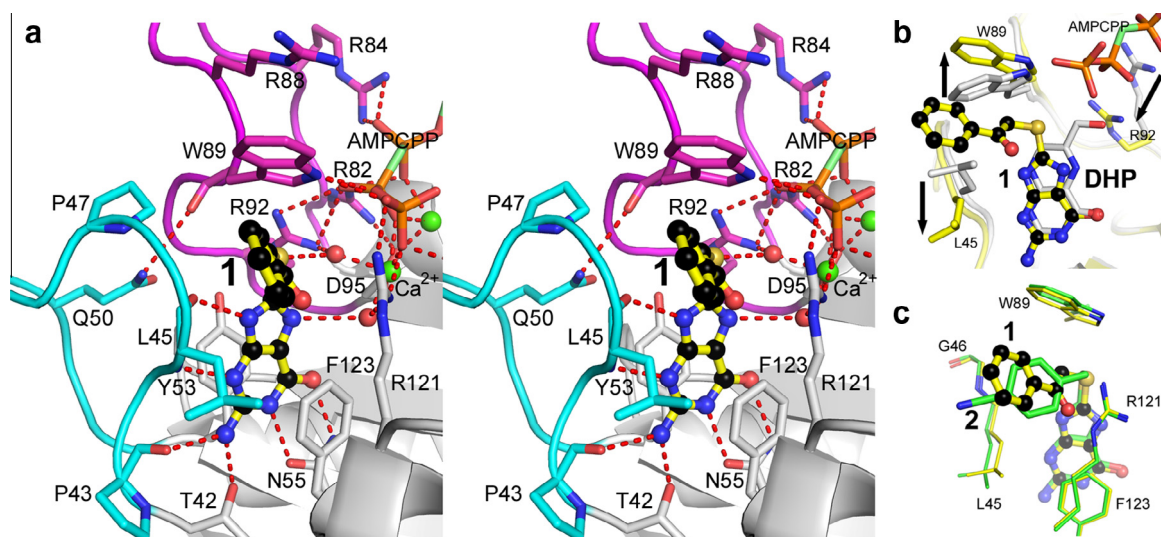


Figure 1. Crystal structures of the HPPK ternary complexes with compounds **1** and **2**. (a) Detailed stereo view of the **1** ternary complex. See text for details of the interaction. The complex contains many hydrogen bonds (dotted red lines) that involve a number of ordered water molecules (red spheres). Loop2 and loop3 that become ordered in the complex are colored cyan and magenta, respectively. Only the phosphate groups (orange/red) of AMPCPP are shown for clarity (the α - β carbon bond is shown in green). (b) Comparison of the **1** (yellow carbons) and DHP (grey carbons) ternary complexes. Note the movements (indicated by arrows) of Leu45, Trp89 and Arg92. (c) Comparison of the **1** and **2** ternary complexes showing the different orientations of the two substituents within the pocket bounded by Leu45 and Trp89.

pocket in much the same way as the pterin ring of DHP. It is sandwiched between Tyr53 and Phe123, and ring oxygen and nitrogen atoms engage in specific hydrogen bonding interactions with the side chains of Thr42 and Asn55, the main chains of Pro43 and Leu45, and a number of structured water molecules. Loop2 and loop3 both adopt ordered structures to facilitate these interactions that closely resemble their conformations in the substrate ternary complex. The substrate ternary complex suggests that substituents at the 8-thio position would not be tolerated because of steric clashes with the side chains of Leu45 and Trp89. However, 8-thio substitution creates a new cryptic binding pocket by an induced fit mechanism in which these side chains rotate to generate the required space (Fig. 1b). Also, the inherent flexibilities of loop2 and loop3 that contain these two residues are exploited by small additional conformational adjustments. Although Trp89 adopts a new conformation, the ring nitrogen atom is still able to form the hydrogen bonding interaction with the γ -phosphate oxygen atoms of AMPCPP that is observed in the substrate ternary complex. The structure of the compound **2** ternary complex is virtually identical to that of **1** apart from the orientation of the substituent within the induced pocket (Fig. 1c).

Movements of Arg82 and Arg92 adjacent to the phosphate groups of the bound ATP play an essential role in HPPK catalysis,^{16,27} and compounds **1** and **2** induce similar conformational changes in these conserved basic residues. In the substrate ternary

complex, Arg84 and Arg92 engage the α - and α/β -phosphates of the nucleotide, respectively, and Arg82 forms a salt bridge with Glu77. However, in the inhibitor structures (Fig. 1a), Arg82 and Arg92 move to form salt bridges with Asp95 and to engage the α - and β -phosphates, respectively, while Arg84 maintains its interaction with the α -phosphate. These movements appear to be related to the absence of the hydroxyl group that is present in DHP and to the ‘pulling’ effect of the substituents at the 8-thio position. Together, these create additional space adjacent to the pterin pocket that becomes occupied by the side chain of Arg92 (Fig. 1b), which then allows Arg82 and Arg84 to relocate into their new positions (Fig. 1a).

2.3. Analysis of 8-substituted-8-thioguanine derivatives

The enzyme end-point assay and the SPR data both suggest that **1** is a marginally better inhibitor of EchHPPK than **2** (Table 1). Although the crystal structures are very similar, the source of this potency appears to be a key interaction in **1** that involves the carbonyl group on the linker between the phenyl and 8-thioguanine moieties (Fig. 1a). Specifically, the carbonyl group stacks onto the guanidinium group of Arg121 that, in turn, forms a stabilizing salt bridge interaction with the γ -phosphate of AMPCPP. The carbonyl group is not present in **2**, and the terminal phenyl group moves further into the pocket to partially stack with Arg121 (Fig. 2a). How-

ever, this movement requires an additional rotation of the Leu45 side chain (Fig. 2a), and appears to result in a less optimal docking with the newly created pocket.

Having established the importance of the carbonyl group within **1**, we synthesized and tested the activities of a number of variants with different substitutions on the phenyl ring. Table 1 shows the 7 derivatives (compounds **3–9**) with comparable activities to **1** and **2**, and Table S3 shows the 7 compounds with significantly reduced activities (compounds **11–17**). Analysis of the latter compounds reveals that extension of the phenyl substituent (**11**), loss of the aromatic ring (**12**), large substitution at the *ortho* position of the phenyl ring (**13**), and changes to the carbonyl-containing linker group (**14–17**) all result in loss of activity. The results of the endpoint inhibition assay shown in Table 1 cannot readily distinguish between the potencies of compounds **1–9**, and we therefore determined their K_D values using SPR and also measured their IC_{50} values by conducting the enzyme assay at increasing concentrations of compound between 0 and 500 μ M (see Section 5 for details). The SPR data and the IC_{50} measurements are shown in Figures S1 and S5, respectively. Overall, small substitutions at the *para* and *meta* positions (**3**, **4**, **5**, **7** and **8**) are preferred over larger *para* substitutions (**6**) and *ortho* substitutions (**9**). To investigate this pattern more systematically, the crystal structures of the ternary complexes with **3**, **7**, **8** and **9** were determined (Tables 2, S1 and S2).

All four ternary complex structures are virtually identical to that of **1**, and the only significant differences occur in the immediate vicinity of the phenyl ring (Fig. 2b–e). In the **3** and **7** ternary complexes (Fig. 2b and c), the *para*-substituents extend directly away from the pocket, and this appears to ‘push’ the phenyl group into the interior of the pocket by ~ 1 Å compared to **1**. This results in a more favorable stacking interaction between the planar carbonyl and the guanidinium group of Arg121, and may explain why the *para* substitutions generally display superior activities. The **8** structure (Fig. 2d) shows that the *meta*-substituent has little effect on the docking conformation, and is able to form a favorable van der Waals interaction with Leu45. Finally, the **9** structure (Fig. 2e) reveals that the *ortho*-methyl group is directly adjacent to Leu45 which is forced to rotate further away compared to the

other structures. This explains the lower activity of **9**, and the much lower activity of **13** in which the *ortho*-substituent is somewhat larger (Table S3). It should be noted that there is a crystallographic caveat to these structural observations, namely, a close contact with an adjacent molecule in the crystal lattice that impacts the *para* substitution more than the *ortho* and *meta* substitutions.

2.4. Further studies on the HPPK pterin-binding pocket

In contrast to previous studies,²⁰ we found that 8-thioguanine (**10**) is a very poor inhibitor of EchHPPK and shows minimal binding by SPR in the presence of AMPCPP (Table 1 and Fig. S1j). This explains why, despite a number of attempts, we have failed to obtain a crystal structure of EchHPPK bound to **10**. It was previously predicted that the sulfur atom in **10** would form a van der Waals interaction with Trp89,²⁰ and our structures of **1**, **2**, **3**, **7**, **8** and **9** have not only confirmed this but revealed the potential for a steric clash. It appears that our inhibitory compounds that contain this scaffold are only able to bind because the substituents ‘pull’ the scaffold away from Trp89 and also rotate the side chain, thereby relieving the steric clash. This in turn suggests that **10** is actually a suboptimal scaffold that compromises the binding of all the compounds that contain it. Given this limitation, we decided to search for alternative scaffolds for optimization.

We first examined 6-thioguanine (**18**) in which the sulfur atom is moved to a position on the scaffold that would not interact with Trp89. Although solubility issues prevented the measurement of a meaningful IC_{50} value, **18** is apparently a far superior inhibitory scaffold than 8-thioguanine based on percent inhibition (Table 3). This was confirmed by SPR that revealed a low μ M K_D value (Table 3) and showed that it binds only in the context of the ternary complex with AMPCPP (Fig. S6a). The crystal structure of the ternary complex (Tables 2 and S2, Figures 3A and S3c) shows that **18** engages the pterin pocket in the same fashion as the 8-thioguanine scaffold, but there is no steric clash with Trp89 and the sulfur atom occupies available space adjacent to Asn55. **18** is a low molecular weight efficient HPPK binder that can be considered a fragment ‘hit’, and its ligand efficiency can be monitored using the ‘Percent Efficiency

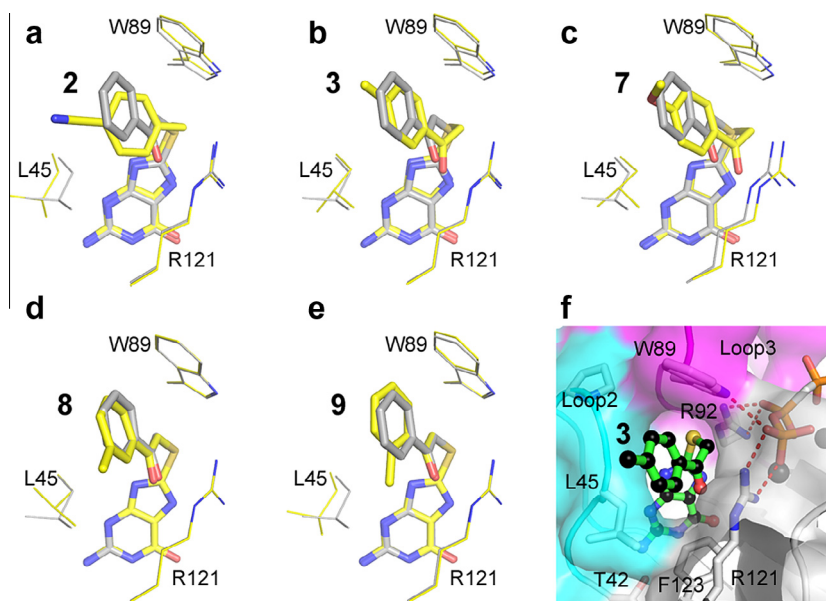


Figure 2. Crystal structures of HPPK ternary complexes with compounds related to **1** (**2**, **3**, **7**, **8** and **9**). In panels a–e, the **1** structure (grey carbons) is superimposed on the compound structure (yellow carbons), and only three key residues are shown for clarity. Panel f shows the **3** complex in a surface representation to emphasize the engagement of the 8-thio substituent within the cryptic pocket created by loop2 (cyan) and loop3 (magenta).

Table 3
Fragments

Compound	Structure	% Inhibition ^a	K _D (μM) ^b	PEI ^c
18		51	18 ± 1	3.05
19		48	38 ± 3	3.18
20		49	18 ± 1	2.97
21		48	7.5 ± 0.2	2.87

^a % Inhibition of enzyme activity was tested at 250 μM of the compound.

^b K_D value was determined by SPR with equilibrium affinity analysis in the presence of 2 μM AMPCPP.

^c Percent Efficiency Index (PEI) was calculated as the percent inhibition (expressed in fraction) at 250 μM of the compound divided by the molecular weight (expressed in kDa) of the inhibitor compound. The PEI value of compound **3** is 2.54.

Index' (PEI)²⁸ metric. This value for **18** (Table 3) confirms the suitability of the molecule for future elaboration.

Next, applying best practices from other fragment-based drug discovery programs,^{29,30} we decided to optimize the **18** scaffold to identify the best starting templates for further elaboration. We did this by conducting a 2D similarity search for new fragments with high Tanimoto similarity to **18** against the NCI database of compounds and applying a molecular weight cutoff of 300 Daltons. 25 fragments were shortlisted, and 17 were able to be obtained from the NCI and verified to be >95% pure using HPLC analysis. Docking simulations using AutoDock showed that they all have the potential to bind within the pterin-binding pocket in a similar manner to **18** (Fig. 3b). When tested, three of these fragments, **19**, **20** and **21** (Table 3), showed inhibitory activities around 50% with PEI values similar to **18**. All three are dihydropurine fragments that also showed AMPCPP-dependent binding by SPR with K_D values comparable to **18** (Table 3 and Figs. S6b-d). Similar to **18**, limited

solubility did not allow the measurement of their IC₅₀ values. **19** and **20** both resemble 8-thioguanine, but with the sulfur atom at the 8-position replaced with a hydrogen atom and a methyl group, respectively, and their improved potencies and abilities to bind EchHPPK in a ternary complex support our notion that the bulky sulfur atom in 8-thioguanine leads to a steric clash with Trp89 when loop3 becomes ordered in the presence of nucleotide.

Compound **21** is distinct from any of the other scaffolds, and we determined the structure of its ternary complex (Tables 2 and S2, Figs. 3c and S3d) to establish its mode of binding. It binds within the pterin pocket, as anticipated, but exploits the available hydrogen bonding architecture in a different way compared to the other scaffolds. The sulfur atom engages the same space as that of **18** adjacent to Asn55, but the side chains of Leu45 and Trp89 adopt different conformations to accommodate the scaffold. Most notably, Trp89 rotates by almost ~120° and the ring nitrogen atom no longer forms a hydrogen bond with the γ-phosphate oxygen atoms of AMPCPP. This rotation of Trp89 appears to be caused by two water molecules (Wat1 and Wat2 in Fig. 3c) that occupy extra available space in the **21** complex and create a new hydrogen bonding constellation involving the γ-phosphate oxygen atoms of AMPCPP and the carbonyl oxygen atoms of Arg88 and Gly90.

3. Discussion

The bacterial enzymes HPPK and DHPS catalyze adjacent steps in the folate biosynthetic pathway, and they each have very specific pockets that engage their pterin substrates. Although the two pockets have different architectures and have apparently evolved independently, our recent demonstration that a small molecule can bind both pockets⁴ suggested that pterin-like scaffolds can be used in parallel to seek potent inhibitors of both enzymes. The successful identification of two HPPK inhibitors from our library of molecules designed to engage the DHPS pterin-binding pocket supports this proposal. The two compounds are structurally related and contain an 8-thioguanine scaffold with two different groups at the 8-thio position. A preliminary SAR analysis of the 8-thio substituent indicated that this series is not suitable for further development, and we showed that the problem is the sulfur atom that hinders the binding of 8-thioguanine within the HPPK pterin pocket. We subsequently identified tighter binding fragment molecules and confirmed by X-ray crystallography that they can specifically engage the pterin pocket without the steric issues experienced by 8-thioguanine.

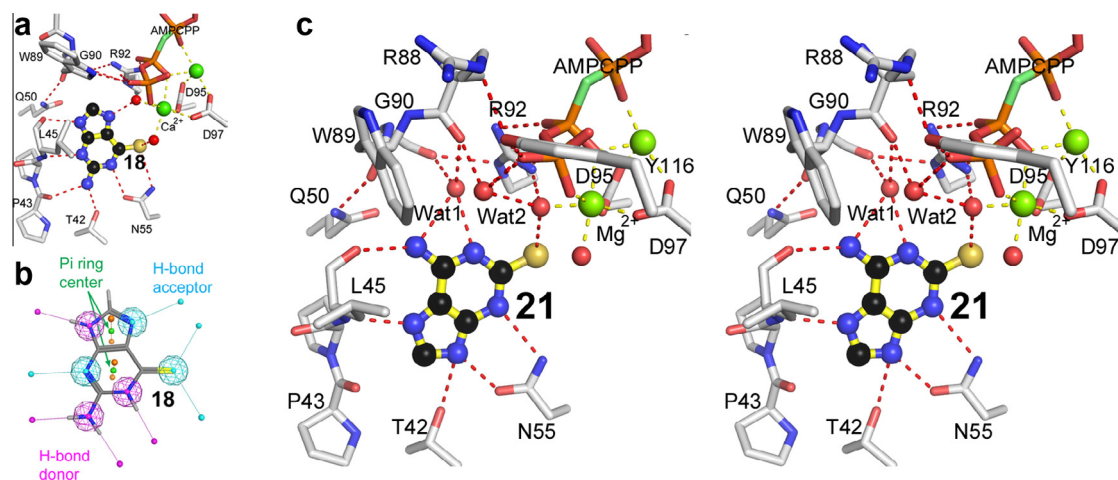


Figure 3. Crystal structures of HPPK ternary complexes with two sulfur-containing inhibitory scaffolds. (a) Compound **18** (6-thioguanine). (b) The chemical fingerprint of **18** in the HPPK pterin-binding pocket in the same orientation as (a). (c) Stereo view of compound **21** in the HPPK ternary complex. Note that the side chains of Leu45 and Trp89 are in different orientations compared to the other reported structures.

Independent studies have previously identified 8-thioguanine as an HPPK inhibitor suitable for development,²⁰ and preliminary attempts to do this were recently reported.²³ These studies, using HPPK from *S. aureus*, showed that 8-thioguanine can bind in the absence of nucleotide, but our SPR data show that binding is minimal both in the absence and presence of nucleotide. In the published structure, 8-thioguanine binds the pterin pocket in the context of a non-physiological crystal dimer with the small molecule at the dimer interface. In addition, the flexible loop3 containing Trp89 was displaced and it was not possible to crystallize the ternary complex with AMPCPP. Our structures have confirmed the prediction²⁰ that the sulfur atom is directly adjacent to Trp89 in the ternary complex. However, the binding of our 8-thioguanine derivatives only appears possible because the 8-position substituents create the necessary space.

Our future goals will be to use these preliminary data to develop more potent inhibitors of HPPK with whole cell activity using structure-based approaches. Our current results have suggested a number of avenues to achieve this that will be pursued. First, we have identified several novel and quite potent pterin pocket binding scaffolds, and each of these will be elaborated into mini libraries for further screening. Second, our analyses of the 8-thioguanine derivatives have provided key information on how these scaffolds can be elaborated to take advantage of a cryptic pocket adjacent to the active site that is induced upon binding. This pocket (Fig. 2f) has in fact been previously identified from earlier structural studies of an HPPK inhibitory molecule that contains the pterin scaffold.⁶ Finally, the nucleoside and triphosphate binding sites are potentially rich unexploited locales for further optimization of our evolving molecules. The build-out of our inhibitors into these adjacent sites offers the possibility of generating tight-binding nucleotide-independent inhibitors. Similar strategies involving the synthesis of bisubstrate analogs (pterin-nucleotide adducts) have already demonstrated the feasibility of this approach for this target.^{7,21,22} We recognize that these nucleotide binding sites are inherently polar and that the build-out process must eventually incorporate strategies for optimizing membrane permeability and cell penetration.

A particular challenge in developing potent inhibitors of HPPK is the functional flexibility of the active site loops and key residues. Our crystal structures have confirmed the inherent plasticity of the HPPK active site locale that even extends to the pterin pocket (Figs. S7 and S8), and inhibitor binding is clearly associated with a considerable entropic penalty as the flexible loops become ordered. This presumably explains why all of our inhibitors only display modest K_D values. However, this provides two advantages that we intend to exploit. First, our low molecular weight inhibitors are essentially fragment molecules, and it has been well established that plasticity within the fragment binding locale can be used to great effect to 'evolve' tight binding derivative molecules.^{29,30} Second, the unavoidable entropic penalty will dictate that enthalpic binding must be optimized in derivative molecules, and this should lead to tight binding molecules with slow off rates.

Antimicrobial antifolate therapeutics that contain a combination of sulfa drugs (DHPS) and dihydrofolate inhibitors have proven to be very effective,³¹ and HPPK/DHPS pterin-based inhibitors offer the possibility of alternate combination therapies. The high conservation of the HPPK and DHPS pterin pockets in all micro-organisms should mean that these therapies have broad spectrum potential that are less prone to resistance mutations. These agents should also be suitable for use in patients with sulfa-allergies and in patient populations with high incidence of sulfa allergies such as those with HIV undergoing prophylaxis to prevent pneumocystis pneumonia.³² To obtain such therapeutics, it is clear that these compounds must be further optimized to enhance target affinity and microbial penetration, and to maximize exposure in the host.

We believe that the structural and biochemical data presented in this study have provided an excellent basis to enable such efforts to move forward rapidly.

4. Conclusions

In summation, the flexibility and druggability of the pterin binding pocket of HPPK has been structurally and biochemically investigated through detailed enzymatic inhibition assays, X-ray crystallography, surface plasmon resonance and computational modeling. These techniques were used to screen a set of compounds originally procured to target the pterin binding site of DHPS, the subsequent enzyme in the folate biosynthetic cascade, which identified 8-substituted-8-thioguanines as potential inhibitors of HPPK. Key to this discovery was that 8-thiosubstitution induced a new cryptic binding pocket adjacent to the pterin binding site, and further analogs were developed to more optimally engage this pocket. Free 8-thioguanine was shown to be a suboptimal pterin pocket binding core, and a series of dihydropurine fragments was identified that should yield more efficient enzyme inhibitors. The structural activity relationships derived from these various molecules, when merged, will facilitate the future design of potent HPPK inhibitors with the potential of being developed into novel antimicrobial therapeutics suitable to combat the rising threats of drug resistant bacteria.

5. Experimental

5.1. Enzyme preparation

The EchHPPK-GST fusion gene was kindly provided by Dr. Honggao Yan (Michigan State University). The EchHPPK-GST fusion enzyme was expressed in *E. coli* and purified as previously described in three steps: (1) GSTrap FF column (Amersham Biosciences), (2) thrombin digestion to remove the GST tag, and (3) size exclusion chromatography.^{27,33}

5.2. Enzyme assay

HPPK activity was determined by measuring unprocessed ATP substrate using the Kinase-Glo Luminescent assay kit (Promega).²⁰ The enzyme activity of HPPK was measured in a reaction mixture of 50 μ l containing 0.75 μ M 6-hydroxymethyl-7,8-dihydropterin hydrochloride (Schircks Laboratories), 0.75 μ M ATP, 100 mM Tris-HCl, pH 8.5, 10 mM MgCl₂, 10 mM BME, 0.01%(V/V) Tween 20, 0.01%(W/V) BSA, 5% DMSO, and 5 ng EchHPPK. Inhibitor compounds were dissolved in DMSO, and inhibition was tested at 250 μ M. After 20 min of incubation at 23 °C, the unprocessed ATP was detected using the Kinase-Glo assay kit with a Multi-Detection Microplate Reader Synergy™ HT (BioTek) according to manufacturer's suggested protocols. The above assay conditions were established after a preliminary optimization procedure to find an ideal compromise between the luminescence signal, the linearity of the reaction, and the reduction in signal caused by the inhibitors. To determine the half maximal inhibitory concentration (IC₅₀) values, HPPK activities were measured in the presence of increasing concentrations of the compounds ranging from 0 to 500 μ M in duplicate. IC₅₀ values were calculated from the dose-response curves using GraphPad Prism (version 5.00).

5.3. Biotinylation of HPPK

HPPK was minimally biotinylated by reaction with EZ-Link Sulfo-NHS-LC-LC-Biotin (Thermo Scientific). The biotin reagent was added to the protein at a 0.5:1 molar ratio, and the reaction was

incubated on ice for 5 h. Unconjugated biotin was removed by processing the samples through two Zeba Spin Desalting Columns (Thermo Scientific) that had been equilibrated with storage buffer (20 mM Tris (pH 8.0), 100 mM NaCl, 10% glycerol). Bovine serum albumin (BSA) was added to the reaction at a final concentration of 0.1 mg/mL immediately prior to processing through the spin columns to improve recovery.³⁴ The biotinylated protein was aliquoted, flash-frozen and stored at -80°C for use in subsequent binding experiments.

5.4. Affinity analysis of compound binding by surface plasmon resonance

SPR experiments were conducted at 20°C using a SensiQ Pioneer optical biosensor (SensiQ Technologies). Neutravidin (Thermo Scientific) was covalently immobilized on a polysaccharide hydrogel-coated gold surface (COOH5 chip; SensiQ Technologies) using routine amine coupling chemistry in immobilization buffer (10 mM HEPES pH 7.4, 150 mM NaCl, 0.005% Tween20). Carboxyl groups on the hydrogel were activated with *N*-ethyl-*N'*-(3-dimethylamino-propyl) carbodiimide (EDC) and *N*-hydroxysuccinimide (NHS), and neutravidin was injected until immobilization levels of ~ 5000 – 7000 RU were achieved. Remaining active sites were blocked by reaction with ethanolamine. The instrument was primed with binding buffer (20 mM Tris pH 8.5, 100 mM NaCl, 10 mM MgCl_2 , 1 mM TCEP, 0.005% Tween20, 10% glycerol, 5% DMSO), and biotinylated HPPK was injected until ~ 3000 – 3700 RU of protein was captured. Unoccupied biotin-binding sites of neutravidin on both the reference and HPPK surfaces were blocked with amine-PEG₂-biotin (Thermo Scientific) to minimize potential non-specific binding by the compounds.³⁵ For the binding of compounds **5**, **6**, **7**, **8**, **10** and **20** to HPPK in the absence of AMPCPP, the data were collected in screening mode (i.e. a single injection at 100 μM). For all other experiments, the compounds were prepared in running buffer as a 3-fold dilution series starting at 100 μM and were injected at a flow rate of 80 $\mu\text{L}/\text{min}$. A series of buffer-only (blank) injections was included throughout the experiment to account for instrumental noise. The data were processed, double-referenced, solvent corrected and analyzed^{35,36} using the software package Qdat (version 2.1.0.21, Biologic Software). The equilibrium dissociation constants were determined by fitting the data to a 1:1 interaction model.

5.5. Crystallographic analyses

Crystals were grown by the vapor diffusion method at 18°C . The protein solution (6.6 mg/ml in 20 mM Tris-HCl, pH 8.0, and 0.1 M NaCl) was incubated with 4 mM AMPCPP (α,β -methyleneadenosine 5'-triphosphate lithium salt, Sigma), 20 mM MgCl_2 , and 1–2 mM compound (final 4% DMSO) to form a complex. An additional 5 mM TCEP (Tris(2-carboxyethyl)phosphine hydrochloride) was added to the complex solutions of compounds **2** and **18**. Initial crystals were identified robotically using the PEGs suite, PEGs II suite, and JCSG+ suite crystallization screening kits (Qiagen), which were manually optimized. The co-crystallization conditions for compounds **1**, **3**, **7**, **8** and **9** are 0.1 M Tris-HCl, pH 8.5, 0.2 M CaCl_2 , and 25% PEG 4 K, in a 1:1 ratio with the protein complex solution. The crystals of compounds **2** and **18** were obtained with the reservoir solution containing 0.1 M HEPES-NaOH, pH 7.5, 0.2 M CaCl_2 , and 25–30% PEG 4 K. The crystal of compound **21** was grown with the reservoir solution that contained 0.1 M sodium cacodylate, pH 6.5, and 1 M tri-sodium citrate. Crystals were cryoprotected with 30% glycerol, and then flash frozen in liquid nitrogen. All diffraction data were collected at the SERCAT beam lines 22-ID and 22-BM at the Advanced Photon Source, and processed using HKL2000.³⁷ Structures were solved by molecular replacement using the EchPPK structure as the search model. Structures were refined and

optimized using PHENIX³⁸ and COOT,³⁹ respectively. Data collection and refinement statistics are summarized in Table 2, and are fully presented in Supplementary Tables S1 and S2 together with the PDB accession codes.

5.6. Fragment optimization

Based on the hit fragment 6-thioguanine (**18**), a 2D chemical similarity search was conducted against the NCI database (265,242 compounds) for fragment-like molecules (Molecular weight cutoff: 300 Da) yielding 25 compounds. The resulting hits were docked into the pterin site receptor derived from EchPPK/6-thioguanine structure using AutoDock 3.05 to find their probable binding modes and binding energies. Out of the 25 compounds, only 17 were actually available at the NCI; these were acquired from the NCI (see below) and their activities were tested against EchPPK.

5.7. Compound procurement

Compounds **1**, **2**, **10** and **18–21** were either obtained from commercial vendors or compound repositories. The details are as follows: **1**, **2**, Scientific Exchange, Inc.; **10**, Ryan Scientific, Inc.; **18**, Sigma-Aldrich Co.; **19–21**, Drug Synthesis and Chemistry Branch, Developmental Therapeutics Program, Division of Cancer Treatment and Diagnosis, NCI.⁴⁰ Compounds **3–9** and **11–17** were synthesized as described below.

5.8. Chemistry

All chemicals and solvents were purchased from Sigma-Aldrich chemical company (St Louis, MO) and used as received. All chemical reactions were tracked by TLC using Silicycle Silica Gel 60F₂₅₄ plates and spots were visualized by UV lamp or I₂ condensation. ¹H NMR spectra were recorded on a 400 MHz Bruker NMR and chemical shifts were reported relative to solvent peak. Analytical RP-HPLC was determined on both a Waters Acquity UPLC-MS equipped with an Acquity BEH C18 column (1.7 μm), flow rate of 0.5 mL/min and a gradient of solvent A (water with 0.1% formic acid) and solvent B (acetonitrile with 0.1% formic acid): 0–0.25 min 97% A; 0.25–3.0 min 3–100% B (linear gradient); 3.0–4.5 min 100% B; 4.5–4.75 min 0–97% A (linear gradient); 4.75–5.0 min 97% A. Purity was monitored by both UV absorbance (monitored at 225–475 nm) and ELSD detection methods. All compounds were found to have >95% purity with the described analytical methods. High resolution mass spectra were determined using a Waters Xevo G2 QTof.

5.8.1. General procedure for the preparation of compounds 3–9 and 12–17

In a round bottom flask equipped with a stir bar was dissolved 2-amino-6-hydroxy-8-mercaptapurine (1–2 mmol, 1.0 equiv) in aqueous sodium hydroxide (0.4 N, 10 mL) and corresponding phenyl substituted 2-bromoacetophenones (1.25–2.5 mmol, 1.25 equiv) dissolved in EtOH (2 mL) was added. The mixtures were stirred for 1 h at room temperature before the solution was neutralized by drop wise addition of HCl (1 N) to yield a precipitate. The precipitate was collected via vacuum filtration, washed with diethyl ether and verified to be pure via LC-MS and ¹H NMR.

5.8.1.1. 2-Amino-8-((2-oxo-2-(*p*-tolyl)ethyl)thio)-1H-purin-6(7H)-one: (3). Yield: 769.5 mg (98%) of off white powder ¹H NMR (400 MHz, DMSO-*d*₆) δ 2.38 (s, 3H), 2.55 (s, 4H), 4.67 (s, 2H), 6.05 (s, 2H), 7.32 (d, *J* = 7.94 Hz, 2H), 7.87–8.00 (m, 2H), 10.57 (s, 1H). ESI-HRMS: *m/z*: calcd: 316.0824 found: 316.0890.

5.8.1.2. 2-Amino-8-((2-(4-hydroxyphenyl)-2-oxoethyl)thio)-1H-purin-6(7H)-one: (4). Yield: 188.2 mg (59.3%) of off white powder. ¹H NMR (400 MHz, DMSO-*d*₆) δ 4.71 (s, 2H), 6.36 (s, 2H), 6.70–6.79 (m, 2H), 7.79–7.88 (m, 2H). ESI-HRMS: *m/z*: calcd: 318.0616 found: 318.0673.

5.8.1.3. 2-Amino-8-((2-(4-fluorophenyl)-2-oxoethyl)thio)-1H-purin-6(7H)-one: (5). Yield: 416.8 (52.2%) of red solid ¹H NMR (400 MHz, DMSO-*d*₆) δ 4.75 (s, 2H), 6.41 (s, 2H), 7.27–7.34 (m, 2H), 8.05 (dd, *J* = 5.63, 8.71 Hz, 2H). ESI-HRMS: *m/z*: calcd: 320.0573 found: 320.0627.

5.8.1.4. 4-(2-((2-Amino-6-oxo-6,7-dihydro-1H-purin-8-yl)thio)acetyl)benzotrile: (6). Yield: 260.2 mg (80%) of brown powder. ¹H NMR (400 MHz, DMSO-*d*₆) δ 4.89 (s, 2H), 6.29 (s, 2H), 8.03–8.06 (m, 2H), 8.15–8.19 (m, 2H), 10.60 (d, *J* = 27.50 Hz, 2H), 12.35–12.64 (m, 1H). ESI-HRMS: *m/z*: calcd: 327.0619 found: 327.0682.

5.8.1.5. 2-Amino-8-((2-(4-methoxyphenyl)-2-oxoethyl)thio)-1H-purin-6(7H)-one: (7). Yield: 278.5 mg (42%) of white powder. ¹H NMR (400 MHz, DMSO-*d*₆) δ 3.87 (s, 3H), 4.82 (d, *J* = 19.12 Hz, 2H), 6.32 (s, 1H), 6.96–7.27 (m, 2H), 8.00 (dd, *J* = 6.36, 8.71 Hz, 2H), 10.48 (s, 1H), 12.53 (s, 1H). ESI-HRMS: *m/z*: calcd: 332.0773 found: 332.0806.

5.8.1.6. 2-Amino-8-((2-oxo-2-(*m*-tolyl)ethyl)thio)-1H-purin-6(7H)-one: (8). Yield: 367.3 mg (46.6%) of red solid. ¹H NMR (400 MHz, DMSO-*d*₆) δ 2.39 (s, 3H), 4.87 (s, 1H), 6.28–6.39 (m, 1H), 7.41–7.52 (m, 2H), 7.81–7.94 (m, 2H), 10.57 (s, 1H). ESI-HRMS: *m/z*: calcd: 316.0824 found: 316.0890.

5.8.1.7. 2-Amino-8-((2-oxo-2-(*o*-tolyl)ethyl)thio)-1H-purin-6(7H)-one: (9). Yield: 233.2 mg (35.2%) of tan powder. ¹H NMR (400 MHz, DMSO-*d*₆) δ 2.37 (s, 3H), 4.71 (s, 2H), 6.33 (s, 1H), 7.28–7.38 (m, 2H), 7.46 (td, *J* = 1.38, 7.57 Hz, 1H), 7.91 (d, *J* = 7.60 Hz, 1H), 10.55 (d, *J* = 42.42 Hz, 1H), 12.69 (d, *J* = 132.88 Hz, 1H). ESI-HRMS: *m/z*: calcd: 316.0824 found: 316.0416.

5.8.1.8. 2-Amino-8-((2-morpholino-2-oxoethyl)thio)-1H-purin-6(7H)-one: (12). Yield: 166.8 mg (43%) of white powder. ¹H NMR (400 MHz, DMSO-*d*₆) δ 3.45 (d, *J* = 4.97 Hz, 3H), 3.49–3.59 (m, 6H), 3.61 (d, *J* = 4.71 Hz, 3H), 4.22 (s, 3H), 6.32 (s, 2H), 10.52 (s, 1H), 12.52 (s, 1H). ESI-HRMS: *m/z*: calcd: 311.0882 found: 311.0907.

5.8.1.9. 2-Amino-8-((2-(2-methoxyphenyl)-2-oxoethyl)thio)-1H-purin-6(7H)-one: (13). Yield: 431.7 mg (65.1%) of off-white powder ¹H NMR (400 MHz, DMSO-*d*₆) δ 3.93 (s, 3H), 4.68 (s, 2H), 6.28 (s, 2H), 6.89–7.39 (m, 2H), 7.47–7.86 (m, 2H), 10.57 (s, 1H), 12.58 (s, 1H). ESI-HRMS: *m/z*: calcd: 332.0773 found: 332.0806.

5.8.1.10. 2-Amino-8-((1-oxo-1-phenylpropan-2-yl)thio)-1H-purin-6(7H)-one: (14). Yield: 194.4 mg (30.8%) of yellow powder. ¹H NMR (400 MHz, DMSO-*d*₆) δ 1.54 (d, *J* = 6.84 Hz, 3H), 5.44 (q, *J* = 6.89 Hz, 1H), 6.35 (s, 2H), 7.52 (t, *J* = 7.74 Hz, 2H), 7.60–7.70 (m, 1H), 7.96–8.06 (m, 2H), 10.68 (s, 1H), 12.66 (s, 1H). ESI-HRMS: *m/z*: calcd: 316.0824 found: 316.0890.

5.8.1.11. 2-Amino-8-((1-oxo-1-(*p*-tolyl)propan-2-yl)thio)-1H-purin-6(7H)-one: (15). Yield: 217.4 mg (26.4%) of yellow powder. ¹H NMR (400 MHz, DMSO-*d*₆) δ 1.53 (dd, *J* = 2.07, 7.01 Hz, 3H), 2.38 (d, *J* = 2.05 Hz, 3H), 5.43 (s, 1H), 6.34 (s, 2H), 7.27–7.43 (m, 2H), 7.91 (dd, *J* = 2.04, 8.33 Hz, 2H), 10.60 (s, 1H),

12.49 (d, *J* = 31.18 Hz, 1H). ESI-HRMS: *m/z*: calcd: 330.0980 found: 330.1039.

5.8.1.12. S-(2-Amino-6-oxo-6,7-dihydro-1H-purin-8-yl) 4-fluorobenzothioate: (16). Yield: 955.0 mg (88%) of white powder. ¹H NMR (400 MHz, DMSO-*d*₆) δ 6.45–6.61 (m, 2H), 7.20–7.46 (m, 2H), 7.89–8.07 (m, 2H), 10.73 (s, 1H), 12.97 (s, 1H). ESI-MS: [M+H]⁺ Found: 306.2.

5.8.1.13. 2-Amino-8-((2-morpholinoethyl)thio)-1H-purin-6(7H)-one: (17). Yield: 335.6 mg (45.3%) of white powder. ¹H NMR (400 MHz, DMSO-*d*₆) δ 2.35–2.47 (m, 4H), 2.61 (t, *J* = 6.88 Hz, 2H), 3.56 (t, *J* = 4.62 Hz, 4H), 6.32 (s, 2H), 10.60 (s, 1H), 12.53 (s, 1H). ESI-HRMS: *m/z*: calcd: 297.1089 found: 297.1153.

5.8.2. General procedure for the preparation of compound 11

To a stirred solution of **16** (1 mmol, 1.0 equiv) in aqueous sodium hydroxide (0.4 N, 10 mL) was added 4-(2-chloroethyl)morpholine (1.25–2.5 mmol, 1.25 equiv) and the mixture stirred for overnight at room temperature. The solution was then neutralized by drop wise addition of HCl (1 N) to yield a precipitate, which was collected via vacuum filtration, washed with diethyl ether and verified to be pure via LC-MS and ¹H NMR.

5.8.2.1. 2-Amino-8-((2-(4-(2-morpholinoethoxy)phenyl)-2-oxoethyl)thio)-1H-purin-6(7H)-one: (11). Yield: 32.6 mg (7.6%) of brown powder. ¹H NMR (400 MHz, DMSO-*d*₆) δ 2.42 (d, *J* = 5.07 Hz, 4H), 2.60 (dt, *J* = 6.42, 30.99 Hz, 2H), 3.53 (t, *J* = 4.51 Hz, 4H), 4.01 (t, *J* = 6.27 Hz, 1H), 4.25 (t, *J* = 6.30 Hz, 1H), 4.70–4.90 (m, 2H), 6.13 (s, 1H), 6.86 (dd, *J* = 2.73, 8.78 Hz, 2H), 7.89 (dd, *J* = 4.31, 7.68 Hz, 2H), 10.76 (s, 1H). ESI-HRMS: *m/z*: calcd: 431.1457 found: 431.1518.

Acknowledgments

This work was supported by National Institutes of Health Grant AI070721 (S.W.W. and R.E.L.), Cancer Center (CORE) Support Grant CA21765, and the American Lebanese Syrian Associated Charities (ALSAC). We thank Zhenmei Li, John Bollinger and the St. Jude Molecular Interactions Core for technical assistance, and Dr. Honggao Yan (Michigan State University) for reagents. Data were collected at Southeast Regional Collaborative Access Team (SER-CAT) 22-ID and 22-BM beamlines at the Advanced Photon Source, Argonne National Laboratory, and we thank SER-CAT staff for their assistance. Supporting SER-CAT institutions may be found at www.ser-cat.org/members.html. Use of the Advanced Photon Source was supported by the U.S. Department of Energy, Office of Science, Office of Basic Energy Sciences, under Contract No. W-31-109-Eng-38.

A. Supplementary data

Supplementary data (X-ray crystallography data collection and refinement statistics, weakly binding compounds, surface plasmon resonance data, selected electron densities, confirmation of Ca²⁺ ions in the HPPK two-metal ATP-binding site, IC₅₀ measurements and plasticity within in the HPPK pterin-binding pocket) associated with this article can be found, in the online version, at <http://dx.doi.org/10.1016/j.bmc.2014.02.022>.

References and notes

- Blakley, R. L. In *Folates and Pterins*; John Wiley and Sons: New York, 1984; Vol. 1, pp 628.
- Bermingham, A.; Derrick, J. P. *BioEssays* **2002**, *24*, 637.

3. Anand, N. In *Burger's Medicinal Chemistry and Drug Discovery*; Wiley-Interscience: New York, 1996; Vol. 2, pp 527–573.
4. Pemble, C. W. t.; Mehta, P. K.; Mehra, S.; Li, Z.; Nourse, A.; Lee, R. E.; White, S. W. *PLoS One* **2010**, *5*, e14165.
5. Hennig, M.; Dale, G. E.; D'Arcy, A.; Danel, F.; Fischer, S.; Gray, C. P.; Jolidon, S.; Muller, F.; Page, M. G.; Pattison, P.; Oefner, C. J. *Mol. Biol.* **1999**, *287*, 211.
6. Stammers, D. K.; Achari, A.; Somers, D. O.; Bryant, P. K.; Rosemond, J.; Scott, D. L.; Champness, J. N. *FEBS Lett.* **1999**, *456*, 49.
7. Shi, G.; Blaszczyk, J.; Ji, X.; Yan, H. *J. Med. Chem.* **2001**, *44*, 1364.
8. Xiao, B.; Shi, G.; Chen, X.; Yan, H.; Ji, X. *Structure* **1999**, *7*, 489.
9. Lawrence, M. C.; Iliades, P.; Fernley, R. T.; Berglez, J.; Pilling, P. A.; Macreadie, I. G. *J. Mol. Biol.* **2005**, *348*, 655.
10. Garcon, A.; Levy, C.; Derrick, J. P. *J. Mol. Biol.* **2006**, *360*, 644.
11. Blaszczyk, J.; Li, Y.; Cherry, S.; Alexandratos, J.; Wu, Y.; Shaw, G.; Tropea, J. E.; Waugh, D. S.; Yan, H.; Ji, X. *Acta Crystallogr. D Biol. Crystallogr.* **2007**, *63*, 1169.
12. Bermingham, A.; Bottomley, J. R.; Primrose, W. U.; Derrick, J. P. *J. Biol. Chem.* **2000**, *275*, 17962.
13. Blaszczyk, J.; Shi, G.; Yan, H.; Ji, X. *Structure* **2000**, *8*, 1049.
14. Shi, G.; Gong, Y.; Savchenko, A.; Zeikus, J. G.; Xiao, B.; Ji, X.; Yan, H. *Biochim. Biophys. Acta* **2000**, *1478*, 289.
15. Li, Y.; Gong, Y.; Shi, G.; Blaszczyk, J.; Ji, X.; Yan, H. *Biochemistry* **2002**, *41*, 8777.
16. Blaszczyk, J.; Li, Y.; Shi, G.; Yan, H.; Ji, X. *Biochemistry* **2003**, *42*, 1573.
17. Blaszczyk, J.; Li, Y.; Wu, Y.; Shi, G.; Ji, X.; Yan, H. *Biochemistry* **2004**, *43*, 1469.
18. Blaszczyk, J.; Shi, G.; Li, Y.; Yan, H.; Ji, X. *Structure* **2004**, *12*, 467.
19. Swarbrick, J.; Iliades, P.; Simpson, J. S.; Macreadie, I. *Open Enzyme Inhib. J.* **2008**, *1*, 12.
20. Chhabra, S.; Dolezal, O.; Collins, B. M.; Newman, J.; Simpson, J. S.; Macreadie, I. G.; Fernley, R.; Peat, T. S.; Swarbrick, J. D. *PLoS One* **2012**, *7*, e29444.
21. Shi, G.; Shaw, G.; Liang, Y. H.; Subburaman, P.; Li, Y.; Wu, Y.; Yan, H.; Ji, X. *Bioorg. Med. Chem.* **2012**, *20*, 47.
22. Shi, G.; Shaw, G.; Li, Y.; Wu, Y.; Yan, H.; Ji, X. *Bioorg. Med. Chem.* **2012**, *20*, 4303.
23. Chhabra, S.; Barlow, N.; Dolezal, O.; Hattarki, M. K.; Newman, J.; Peat, T. S.; Graham, B.; Swarbrick, J. D. *PLoS One* **2013**, *8*, e59535.
24. Yun, M. K.; Wu, Y.; Li, Z.; Zhao, Y.; Waddell, M. B.; Ferreira, A. M.; Lee, R. E.; Bashford, D.; White, S. W. *Science* **2012**, *335*, 1110.
25. Xiao, B.; Shi, G.; Gao, J.; Blaszczyk, J.; Liu, Q.; Ji, X.; Yan, H. *J. Biol. Chem.* **2001**, *276*, 40274.
26. Li, G.; Felczak, K.; Shi, G.; Yan, H. *Biochemistry* **2006**, *45*, 12573.
27. Li, Y.; Wu, Y.; Blaszczyk, J.; Ji, X.; Yan, H. *Biochemistry* **2003**, *42*, 1581.
28. Abad-Zapatero, C.; Metz, J. T. *Drug Discovery Today* **2005**, *10*, 464.
29. Hajduk, P. J.; Greer, J. *Nat. Rev. Drug Disc.* **2007**, *6*, 211.
30. Congreve, M.; Chessari, G.; Tisi, D.; Woodhead, A. J. *J. Med. Chem.* **2008**, *51*, 3661.
31. Masters, P. A.; O'Bryan, T. A.; Zurlo, J.; Miller, D. Q.; Joshi, N. *Arch. Intern. Med.* **2003**, *163*, 402.
32. Merali, S.; Zhang, Y.; Sloan, D.; Meshnick, S. *Antimicrob. Agents Chemother.* **1990**, *34*, 1075.
33. Hevener, K. E.; Yun, M. K.; Qi, J.; Kerr, I. D.; Babaoglu, K.; Hurdle, J. G.; Balakrishna, K.; White, S. W.; Lee, R. E. *J. Med. Chem.* **2010**, *53*, 166.
34. Papalia, G.; Myszka, D. *Anal. Biochem.* **2010**, *403*, 30.
35. Giannetti, A. M. *Methods Enzymol.* **2011**, *493*, 169.
36. Myszka, D. G. *J. Mol. Recognit.* **1999**, *12*, 279.
37. Otwinowski, Z.; Minor, W. *Methods Enzymol.* **1997**, *276*, 307.
38. Adams, P. D.; Grosse-Kunstleve, R. W.; Hung, L. W.; Ioerger, T. R.; McCoy, A. J.; Moriarty, N. W.; Read, R. J.; Sacchettini, J. C.; Sauter, N. K.; Terwilliger, T. C. *Acta Crystallogr. D Biol. Crystallogr.* **2002**, *58*, 1948.
39. Emsley, P.; Cowtan, K. *Acta Crystallogr. D Biol. Crystallogr.* **2004**, *60*, 2126.
40. Hergenrother, P. J. *Curr. Opin. Chem. Biol.* **2006**, *10*, 213.